Liquid Crystals
Publication details, including instructions for authors and subscription information:
http://www.informaworld.com/smpp/title~content=t713926090

Theory of the Nematic-Isotropic Transition in a Restricted Geometry

A. Poniewierski[a]; T. J. Sluckin[b]
[a] Polish Academy of Sciences, Institute of Physical Chemistry, Warsaw, Poland [b] Faculty of Mathematical Studies, University of Southampton, Southampton, England

To cite this Article Poniewierski, A. and Sluckint, T. J.(1987) 'Theory of the Nematic-Isotropic Transition in a Restricted Geometry', Liquid Crystals, 2: 3, 281 — 311
To link to this Article: DOI: 10.1080/02678298708086677
URL: http://dx.doi.org/10.1080/02678298708086677

LIQUID CRYSTALS, 1987, VOL. 2, NO. 3, 281–311

Theory of the nematic–isotropic transition in a restricted geometry

by A. PONIEWIERSKI
Institute of Physical Chemistry, Polish Academy of Sciences,
01-224 Warsaw, Poland

T. J. SLUCKIN†
Faculty of Mathematical Studies, University of Southampton,
Southampton SO9 5NH, England

(*Received 25 September 1986; accepted 9 January 1987*)

We discuss, using a Landau–de Gennes formalism, the nematic–isotropic transition temperature for a system placed between two parallel plates, subject to identical homeotropic or homogeneous boundary conditions at each plate. The temperature at the phase transition may increase or decrease as the inverse sample thickness, D^{-1}, increases, depending on the nature of the boundary conditions. In all cases the transition terminates at a critical point for sufficiently large D^{-1}, beyond which the nematic and isotropic phases are no longer distinct. The phase transition temperature is well described by a liquid crystal analogy of the Kelvin equation which can be generalized to give an exact Clausius–Clapeyron relation. Under many circumstances the system behaves from a thermodynamic point of view as though it were in a bulk ordering field. The finite geometry restricts the growth of nematic or isotropic wetting films. We discuss the disjoining pressure experiment of Horn, Israelachvili and Perez [15]. Finally we place our work in the context of recent progress in the statistical mechanics of surfaces and systems in restricted geometries.

1. Introduction

The singularities in thermodynamic quantities which are associated with phase transitions in physical and chemical systems only occur in the so-called *thermodynamic limit*, that is, in the limit of infinitely large systems. If system size is restricted in any way, either as a result of the presence of surfaces, or because the system only has finite extent in one or more directions, these singularities are profoundly affected. Their position in the phase diagram may change, new singularities may occur, and the singularities themselves may cease to be. Particular cases of such systems are semi-infinite systems, with one wall, and systems which are infinite in two dimensions but of finite extent in a third; these systems have two walls. Such systems are sufficiently infinite that thermodynamic singularities do occur and sufficiently finite that qualitatively new phenomena also occur.

We have ourselves recently made a theoretical study of nematic liquid crystals in a semi-infinite system [1, 2], and in this paper we extend our study to deal with the two-wall problem. In the liquid crystal context the pioneer of such investigations was Sheng [3]. He studied a semi-infinite sample of nematic liquid crystal in contact with a wall which exerts an ordering potential on the nematic. Under some circumstances a

† Temporary address until September 1988: Institut Laue–Langevin, 156X, 38042 Grenoble Cedex, France.

separate first-order phase transition occurs at the wall, at a temperature slightly above the bulk nematic–isotropic phase transition T_{NI}, and at which orientational ordering occurs close to the wall. In fact, as observed by ourselves [1, 2] and others [4] this so-called boundary layer phase transition is none other than the prewetting transition, a rather general phenomenon occurring when two critical phases are influenced by a third non-critical phase [5]. Sheng also studied a finite size nematic sample between two parallel ordering walls. The phase transition between the disordered isotropic phase and the ordered nematic phase is shifted slightly to higher temperatures. The coexistence curve has its own critical point for some critical value of the thickness. In addition, features of the semi-infinite system phase diagram are preserved. The boundary layer phase transition can occur, although it is rather insensitive to sample thickness D.

There has also been recent experimental work. Kuzma and Labes [6] studied the thermodynamics of a liquid crystal in a cylindrical pore and found that the transition temperature dropped slightly as the pore size was reduced. Yokoyama *et al.* [7] used the birefringence method to study thin nematic films bounded by solid substrates, and their results are consistent to some extent with Sheng's picture. They observed a shift in the transition temperature and there is evidence that the transition becomes continuous at a critical point when the nematic film is still as thick as a few thousand Ångstroms. However, in contradiction with Sheng's study the transition temperature shifted either upward or downward, depending both on the type of nematic and on the type of substrate.

In this paper we study the consequences of the Landau–de Gennes theory of the nematic confined between two walls. We extend somewhat the model of Sheng in order to discuss disordering as well as ordering walls. In the Landau form the theory is in fact applicable to any first-order phase transition in a restricted geometry, in particular magnetic systems and the liquid–gas transition. Such problems have been studied for many years and there has recently been a resurgence of interest associated with the progress made in understanding wetting and spreading phenomena. Kelvin, in the last century, used a thermodynamic argument to derive the shift in the saturated vapour pressure of a vapour in a pore [8]. We shall make the analogous thermodynamic argument, but also be interested in the limits to such arguments. More recently Nakanishi and Fisher [9] were interested in the effect of plate geometry on the liquid–vapour critical point. Their arguments demonstrate that a critical point is expected for a sufficiently thin sample for a system undergoing a first-order phase transition. Lipowsky and Gompper [10] and Sornette [11] have looked at a Landau model between purely disordering plates, and have in particular concentrated on the asymptotic regime of large sample thicknesses. In our work we present calculations over the whole range of D, and for the more generic case of walls which have both ordering and disordering terms. We also discuss the asymptotic regime, which is extremely useful in checking approximate formulae for critical parameters. In addition a number of authors have recently studied the phenomenon of capillary condensation [12], which is essentially the same phenomenon as that which we discuss.

A related phenomenon which can be examined theoretically using the Landau–de Gennes formalism is that of the so-called structural force between two solid walls, the region between which is filled with fluid. This force, sometimes also known as the disjoining force or pressure, exists because each wall independently affects the fluid structure close to it; the presence of the other wall changes this effect slightly, and hence changing the separation affects the free energy. Interest in this phenomenon goes back many years [13]. More recently, Perez *et al.* [14] have made a thermodynamical study

of a liquid crystal system placed between two walls, emphasizing the structural force, and Horn *et al.* [15] have carried out an experimental study of such a system.

The paper is arranged as follows. In §2 we set the scene by deriving various thermodynamic relations which are useful in the development of the theory. In §3 we describe the model. In §4 we explain in principle how the model is solved, and describe how some crucial quantities which crop up in the solution of the model are related to the thermodynamics. In §5, which is of more theoretical interest, we examine asymptotic properties of the model in the large slab thickness limit. In §6 we give the results of the calculation of the nematic–isotropic phase diagram as a function of temperature and slab thickness. We also compare the predictions of the theory for the critical parameters with a simpler heuristic theory, and thus relate this finite size transition to the nematic–isotropic transition in an ordering field. We also make some comments about the relation of the theory to experimental work. In §7 we concentrate on the predictions of the theory for the structural forces between the two walls. Finally in §8 we make some concluding remarks. Although the model is very simple, the calculations are rather long-winded and most of the technical detail of the calculations has been relegated to the two Appendices.

2. Thermodynamics

In this section we discuss various elementary thermodynamical considerations which it will be useful to bear in mind during our discussions of the microscopic model studied in subsequent sections. Although in principle the microscopic model can allow for the presence of a finite magnetic field which has an ordering effect on a nematogen, we shall confine our discussion in this section to the zero magnetic field case.

We first discuss the shift in transition temperature in a system of thickness D. The grand thermodynamic potential Ω is a suitable free energy for this system (the chemical potential μ is supposed fixed). Per unit area, in the simplest approximation, this is given by

$$\frac{\Omega}{A} = -pD + 2\gamma, \tag{1}$$

where γ is the surface free energy, p is the bulk pressure and A is the area. We denote the surface free energies of the nematic and isotropic phases by γ_N, γ_I, respectively, and the Young–Laplace surface tension formula yields

$$\gamma_I = \gamma_N + \gamma_{NI}\cos\theta, \tag{2}$$

where θ is the contact angle at a nematic–isotropic–wall line of contact, and γ_{NI} is the surface tension at the nematic–isotropic interface. We denote the pressures in the isotropic and nematic phases at temperature T by $p_I(T)$ and $p_N(T)$, respectively. The bulk coexistence temperature T_{NI} is defined by

$$p_I(T_{NI}) = p_N(T_{NI}). \tag{3}$$

In the finite thickness sample the phase transition occurs at $T_{NI}(D) = T_{NI} + \Delta T_{NI}(D)$. At this temperature $\Omega_N = \Omega_I$, or

$$-p_N(T_{NI}(D)) + \frac{2\gamma_N}{D} = -p_I(T_{NI}(D)) + \frac{2\gamma_I}{D}. \tag{4}$$

The shift is small, so

$$p_N(T_{NI}(D)) = p_N(T_{NI}) + \frac{\partial p_N}{\partial T}(T_{NI})\Delta T_{NI}(D),$$
$$= p_N(T_{NI}) + S_N(T_{NI})\Delta T_{NI}(D), \quad (5)$$

where S_N is the entropy per unit volume of the nematic phase at T_{NI}, and a similar equation obtains for p_I. Substituting equation (5) into equation (4), we obtain

$$-S_N\Delta T_{NI} + \frac{2\gamma_N}{D} = -S_I\Delta T_{NI} + \frac{2\gamma_I}{D}, \quad (6)$$

or

$$\Delta T_{NI} = \frac{2(\gamma_I - \gamma_N)T_{NI}}{LD}, \quad (7)$$

where

$$L = T_{NI}(S_I - S_N)$$

is the latent heat per unit volume at the bulk nematic–isotropic transition. Variations of this equation date back to Kelvin [8] and we call this the Kelvin approximation [16]. A trivial consequence of equation (7), using equation (2), is that

$$\Delta T_{NI} = \frac{2\gamma_{NI}\cos\theta T_{NI}}{LD}, \quad (8)$$

and thus if $\cos\theta > 0$ then T_{NI} is increased, whereas if $\cos\theta < 0$ then T_{NI} is decreased, as might be expected intuitively.

However, the formulae (7) and (8) are only approximate. They ignore the interaction between the walls. Equation (1) must be supplemented in order to take this into account. We then obtain

$$\frac{\Omega}{A} = -pD + 2\gamma + \Xi(D), \quad (9)$$

where all wall interaction effects are taken account of by the interaction potential $\Xi(D)$, which must be calculated microscopically. However,

$$-\frac{1}{A}\left(\frac{\partial\Omega}{\partial D}\right)_{T,\mu} = p - \frac{\partial\Xi}{\partial D} = p + \pi_D \quad (10)$$

defines the *disjoining pressure* or *disjoining force* [13], π_D. The quantity π_D is the force required, per unit area, to keep two walls a distance D away from each other when the whole system is immersed in an infinite bath of the same fluid as is between the walls. The infinite bath provides the pressure p, but the extra pressure π_D must be supplied mechanically.

The thermodynamical potential appropriate at constant disjoining pressure is Ψ, where

$$\frac{\Psi}{A} = \frac{1}{A}\left[\Omega - D\frac{\partial\Omega}{\partial D}\right] = 2\gamma + D\pi_D + \Xi,$$
$$= 2\tilde{\gamma}(D). \quad (11)$$

This obeys the equation

$$\left(\frac{\partial\tilde{\gamma}}{\partial D}\right)_{\pi_D} = 0. \quad (12)$$

Then $\tilde{\gamma}(D)$ is the surface tension per wall on the two-wall system, and in some sense is the finite D analogue of γ.

A more exact analogue of equation (7) can now be calculated. This equation will be the Clausius–Clapeyron equation for the nematic-isotropic coexistence curve with changing D. If $T_{NI}(D)$ and $T_{NI} + dT_{NI}(D + dD)$ are neighbouring points on the coexistence curve, we have, following the usual Clausius–Clapeyron-type arguments,

$$\Delta\Omega = \Omega_N - \Omega_I = 0 \tag{13}$$

and

$$\frac{1}{A}\frac{\partial\Delta\Omega}{\partial D}dD + \frac{1}{A}\frac{\partial\Delta\Omega}{\partial T}dT_{NI} = 0. \tag{14}$$

Following the argument of equations (6) and (7),

$$\frac{1}{A}\frac{\partial\Delta\Omega}{\partial T} = D\frac{\tilde{L}(D)}{T_{NI}(D)}, \tag{15}$$

where $\tilde{L}(D)$ is the latent heat per unit volume in the finite system. Also from equation (11), and using equation (13),

$$\frac{1}{A}\frac{\partial\Delta\Omega}{\partial D} = \frac{2}{D}(\tilde{\gamma}_I - \tilde{\gamma}_N). \tag{16}$$

Combining the results in equations (14)–(16) we obtain

$$\frac{\Delta T_{NI}}{\Delta D} = \left.\frac{dT_{NI}(D)}{dD}\right)_{\text{coexistence curve}},$$

$$= \frac{2}{D^2}\frac{(\tilde{\gamma}_N - \tilde{\gamma}_I)}{\tilde{L}(D)}T_{NI}(D), \tag{17}$$

as the equation of the coexistence curve. This is the natural generalization of the Kelvin equation (7) but is now in its exact differential form. We make use of this equation to calculate coexistence curves in our model calculations. Taking the limit $D = \infty, \tilde{\gamma} = \gamma, \tilde{L} = L$ reproduces equation (7). The formula applies so long as a true phase transition does occur.

Finally, in this section, we discuss the phenomenon of capillary condensation. If there were merely one wall, the potential at the wall might favour either phase. When the contact angle $\theta = 0$ the nematic phase is favoured, when $\theta = \pi$ the isotropic phase is favoured, and intermediate values of θ apply to intermediate situations. As has been much discussed recently [4], $\theta = 0$ and $\theta = \pi$ are special situations in that *complete* wetting occurs. We discuss, for definiteness, the $\theta = 0$ case. The nematic phase is then so favoured that as the thermodynamic conditions for nematic–isotropic coexistence are approached a layer of nematic phase forms at the wall, and the thickness of this layer *diverges* as the bulk phase transition is approached. How does this phenomenon generalize to the two-wall situation, where the surface layer is precluded from divergence by the finite thickness of the sample?

The answer to this question depends on the thickness of the sample. Recall, from equation (8), that the phase transition occurs at a higher temperature than in the bulk. The shift in phase transition temperature is $T_{NI} \sim D^{-1}$. Now, for short-ranged surface forces, the thickness of the nematic layer at the wall is given by [5] $H \sim \ln|T_{NI}|$. For a sufficiently thick sample, T will be small, $D \gg H$, and the phase transition will occur *before* the nematic layer has had a chance to grow thick. Indeed,

at each wall the maximum thickness of the nematic layer, before the bulk transition takes place, will be $H \sim \ln D$. This is the phenomenon of capillary condensation. On the other hand for a thin sample, the Kelvin equation (8) suggests a phase transition at a temperature at which the nematic layer thickness at the walls is already larger than the sample thickness. Then we expect no sharp transition. Somewhere in between there will be a critical point. We expect our model calculations to conform to these general observations, and we shall be interested in features of the transition under these circumstances.

3. Model

We consider a nematic sample between two parallel walls placed at $z = 0$ and $z = D$ respectively, and unbounded in the xy plane. The nematic is assumed to be subject to homeotropic boundary conditions (i.e. with its director perpendicular to the walls), although our results may be partly applicable to the case when the nematic is subject to identical homogeneous boundary conditions at each wall (i.e. each plane has an identical easy axis in the xy plane), in which case the system is dominated by the behaviour of the order parameter along this direction. This restriction enables us to assume that the nematic director is uniform throughout the sample. We also ignore nematic density variations in the sample. Thus the only variable depending on z is the nematic order parameter $Q(z) = Q_{zz}(z)$. Following Sheng [3] we take the free energy density in the Landau–de Gennes form

$$\mathscr{F} + L\left(\frac{dQ}{dz}\right)^2 = \mathscr{F}_0 + \tfrac{3}{4}AQ^2 - \tfrac{1}{4}BQ^3 + \tfrac{9}{16}CQ^4 - \tfrac{1}{2}\chi_a H^2 Q + L\left(\frac{dQ}{dz}\right)^2, \quad (18)$$

where $A = A'(T - T^*)$, B and C are temperature-independent parameters, $\chi_a > 0$ is the anisotropic part of the magnetic susceptibility, and H is a uniform magnetic field along the z axis. It is convenient to deal in dimensionless quantities, and in order to do this we introduce a dimensionless order parameter $\eta = (C/B)Q$, and divide $\mathscr{F}$ by B^4/C^3, to obtain [17]

$$F(\eta) = (\mathscr{F} - \mathscr{F}_0)/(B^4/C^3) = \tfrac{3}{4}t\eta^2 - \tfrac{1}{4}\eta^3 + \tfrac{9}{16}\eta^4 - h\eta, \quad (19)$$

where F, $t = AC/B^2$ and $h = \frac{1}{2}\chi_a H^2 C^2/B^3 > 0$ are the dimensionless free energy density, temperature and ordering field respectively. The bulk phase diagram resulting from this free energy has been much studied [17, 18]; however it is useful to recapitulate its basic features.

At temperatures $t > t_c = \frac{1}{18}$ there is just one phase. At temperatures lower than this there are two phases: a low field paranematic phase (at zero field this becomes the isotropic phase) and a high field nematic phase. The coexistence line terminates at a critical point at t_c, $h_c = \frac{1}{324}$, $\eta_c = \frac{1}{4}$. It is linear in the (t, h) plane:

$$h - h_c = (t - t_c)/6, \quad (20)$$

and

$$\eta_p - \eta_c = -2(h_c - h)^{1/2}, \quad (21)$$

$$\eta_N - \eta_c = 2(h_c - h)^{1/2}. \quad (22)$$

Thus at zero magnetic field we have the usual isotropic–nematic transition at $t_{NI} = \frac{1}{27}$, $\eta_p = 0$, $\eta_N = \frac{2}{9}$. Below t_{NI} only the nematic phase exists.

The total dimensionless free energy functional per unit area has the form

$$\phi(\eta) = \xi^{-1} \int_0^D \left[F(\eta) + \xi^2 \left(\frac{d\eta}{dz} \right)^2 \right] dz + \int_0^D V_s(\eta)[\delta(z) + \delta(z - D)]dz, \quad (23)$$

where $\xi = (LC/B)^{1/2}$ is the nematic correlation length, and the second integral gives the surface contribution to the free energy. We assume, as in our previous work [1, 2], the surface potential due to the walls is a contact potential, of zero range, and that it consists of two terms

$$V_s(\eta) = -h_1\eta + \frac{1}{2}g\eta^2. \quad (24)$$

The first term is responsible for surface-induced order ($h_1 > 0$), and the second term for surface-induced disorder ($g > 0$). From a microscopic point of view, the second term is a result of the fact that molecules close to an interface have fewer nearest neighbours than in the bulk. Sheng [1] considered only the first term, although other workers have studied surface-induced disorder [10, 11, 19]. To understand the full range of possible behaviours it is necessary to consider both terms. The equilibrium profile $\eta(z)$ results from the minimization of $\phi\{\eta(z)\}$. This yields the Euler–Lagrange equation

$$2\xi^2 \left(\frac{d^2\eta}{dz^2} \right) = F'(\eta), \quad (25)$$

together with boundary conditions

$$2\xi \left(\frac{d\eta}{dz} \right)_{z=0} = V_s'(\eta)|_{z=0}, \quad (26a)$$

$$2\xi \left(\frac{d\eta}{dz} \right)_{z=D} = -V_s'(\eta)|_{z=D}. \quad (26b)$$

Although this model is very simple, it contains an extremely rich set of behaviours, and the procedure required to solve the model is rather detailed. We discuss the method of solution and the results in the following sections.

4. Solution of model: general considerations

In this section we give a general outline of the procedure required to solve the model introduced in the last section, and make contact between properties of the model and the thermodynamics discussed in §2.

We start with the basic equations of the model, equations (25) and (26). A crucial physical point to note is that the system is symmetric about $z = D/2$, from which it follows that $(d\eta/dz)_{D/2} = 0$. Thus integration of equation (25) yields

$$\xi^2 \left(\frac{d\eta}{dz} \right)^2 = F(\eta) - F(\eta_m), \quad (27)$$

where $\eta_m = \eta(z = D/2)$ is the order parameter at the middle of the sample. The quantities η_m and $F(\eta_m)$ have considerable importance in the theory.

Equations (27) and (23) can be combined to yield an explicit expression for the free energy per unit area

$$\phi = 2\sigma + \left(\frac{D}{\xi}\right) F(\eta_m), \tag{28}$$

where

$$\sigma = \pm 2 \int_{\eta_0}^{\eta_m} \sqrt{[F(\eta) - F(\eta_m)]}\, d\eta + V_s(\eta_0); \tag{29}$$

here the signs +, − correspond, respectively, to a profile increasing or decreasing at $z = 0$, and $\eta_0 = \eta(z = 0)$. Now we can treat ϕ as a function of η_0 and η_m, which should be minimized with respect to these variables. The minimization with respect to η_0 gives

$$\pm 2\sqrt{[F(\eta_0) - F(\eta_m)]} = V_s'(\eta_0), \tag{30}$$

which is consistent with the result we would obtain by combining equations (27) and (26). The minimization with respect to η_m leads to a relation between η_0, η_m, and D, namely

$$D/\xi = \pm 2 \int_{\eta_0}^{\eta_m} \frac{d\eta}{\sqrt{[F(\eta) - F(\eta_m)]}}. \tag{31}$$

If $D \to \infty$ then η_m tends to the bulk order parameter of the infinite system η_b and we recover the semi-infinite sample problem with σ being the wall–nematic or wall–paranematic surface tension. For finite D, on the other hand, the parameters η_0 and η_m are coupled and we have to solve equations (30) and (31) to find them as a function of D, t and h.

From a physical point of view D is the independent variable, and we wish to solve for $\eta_0(D)$ and $\eta_m(D)$. However, in the context of equations (30) and (31) it is clear that if η_0 and η_m are chosen as the independent variables then equation (31) provides an explicit expression for $D(\eta_0, \eta_m)$. The quantities η_0 and η_m are connected by equation (30), which can be recast as

$$F_m(\eta_0) = F(\eta_m) = F(\eta_0) - \tfrac{1}{4}[V_s'(\eta_0)]^2. \tag{32}$$

In this equation it is clear that if η_m is treated as the independent variable, η_0 is an ambiguous function of η_m. On the other hand if η_0 is regarded as the independent variable, then $F_m(\eta_0) = F(\eta_m)$ is well defined. The solution of this equation for $\eta_m(\eta_0)$ is not in fact unique; indeed there may be up to four solutions. The physical solution, however, must obey two further conditions, and this does impose uniqueness. We are thus able to establish a functional relationship $D(\eta_0)$. The conditions are

$$(\eta_m - \eta_0) V_s'(\eta_0) \geqslant 0, \tag{33}$$

and

$$F(\eta) - F(\eta_m) \geqslant 0 \quad \text{for} \quad \min(\eta_0, \eta_m) \leqslant \eta \leqslant \max(\eta_0, \eta_m). \tag{34}$$

Equation (33) follows directly from equations (26); $(\eta_m - \eta_0)$ has the same sign as $(d\eta/dz)_{z=0}$, and hence the same sign as $V_s'(\eta_0)$. Equation (34) is merely the condition that equation (27) is satisfied for all physical η, i.e. all those η lying between η_0 and η_m.

Having shown that η_m is a single-valued function of η_0, we proceed in the following way.

(i) We determine the physical regions of η_0, using the inequality

$$F_m = F(\eta_0) - \tfrac{1}{4}[V_s'(\eta_0)]^2 > \min F(\eta). \tag{35}$$

No solutions for η_m exist if equation (30) is not satisfied.

(ii) We calculate

$$D(\eta_0) = D(\eta_0, \eta_m(\eta_0)) \tag{36}$$

using equation (31).

(iii) We seek solutions to the equation

$$D = D(\eta_0). \tag{37}$$

(iv) We isolate the stable solutions of equation (37). The stability conditions are most conveniently written as

$$F_m'(\eta_0)/V_s'(\eta_0) < 0, \tag{38}$$

$$D'(\eta_0)/F_m'(\eta_0) < 0. \tag{39}$$

We postpone the derivation of these inequalities to Appendix 1.

(v) Finally we find the equilibrium values of η_0 and η_m, corresponding to the absolute minimum of $\phi(\eta_0, \eta_m)$.

4.1. *Thermodynamic properties of the model*

At this stage it will be useful, even before we solve the model by carrying out the set of procedures just outlined, to make contact between the quantities occurring in the model and the general thermodynamic considerations described in §2.

The relevant normalized surface free energy in our model system can be rewritten from equation (28) as

$$\phi = 2\sigma + (D/\xi)F(\eta_b) + (D/\xi)(F(\eta_m) - F(\eta_b)). \tag{40}$$

We can compare this to the thermodynamic expression for the grand thermodynamic potential, Ω, obtained by combining equations (9) and (11) to give

$$\Omega = 2\tilde{\gamma} - Dp - D\pi_D. \tag{41}$$

We identify $F(\eta_b)$ with $-p$, the free energy per unit area of a system of thickness D immersed in the bulk system. The disjoining pressure π_D can now be identified with $-(F(\eta_m) - F(\eta_b))$, and the surface free energy σ can be identified with the thermodynamic quantity $\tilde{\gamma}$. We also note that π_D is the force per unit area required to hold the plates at a distance D apart. The work required to expand the system from a thickness D to a thickness $D + dD$ is

$$\begin{aligned} dW &= \pi_D\, dD \\ &= -\left(\frac{\partial \Omega}{\partial D}\right)_p dD. \end{aligned} \tag{42}$$

Mechanical stability demands that [15]

$$\pi_D(dD + dD) < \pi_D(D), \tag{43}$$

or equivalently

$$\frac{d\pi_D}{dD} < 0. \tag{44}$$

This is a condition on the *physical accessibility* of the system of thickness D, which is produced by supplying physically the force π_D. At a given π_D the system will *slip* through a region where $(d\pi_D/dD) < 0$.

5. Asymptotic behaviour

In this section, before investigating in detail the function $D(\eta_0)$, we find it useful to extract as much information as possible about the large D behaviour of the finite thickness system by carrying out an analysis of its asymptotic behaviour in this regime. We shall first discuss the behaviour, at fixed t, of the quantities $\eta_m(D)$ and $\eta_0(D)$. This analysis gives some further insight into the Kelvin equation for the temperature shift of the phase transition, discussed in §2. We then discuss some aspects of the ordering phase transition at finite D.

At large D we may suppose that η_m is close to $\eta_b = \eta_m(D = \infty)$, and that η_0 is also only slightly perturbed. D, η_0 and η_m are related through equation (31). The principal contribution to this integral comes in the region of η close to η_m. In this regime $F(\eta)$ can be expanded in the following way.

$$F(\eta) - F(\eta_m) \cong \frac{1}{2}\left(\frac{\partial^2 F}{\partial \eta^2}\right)_{\eta_b} [(\eta - \eta_b)^2 - (\eta_m - \eta_b)^2]. \tag{45}$$

Substituting equation (45) into equation (31) yields the asymptotic expression

$$\eta_b - \eta_m \sim \pm \exp\left\{-\frac{1}{2}\left[\frac{1}{2}F''(\eta_b)\right]^{1/2} D/\xi\right\}. \tag{46}$$

For $h = 0$ and $t = t_{NI}$, $\eta_b = 0$ or $\eta_b = \eta_N = \frac{2}{3}$, and $[\frac{1}{2}F''(\eta_b)]^{1/2} = \frac{1}{6}$. We may show in a straightforward way, using equations (29) and (32), that $\eta_0(D)$ and $\sigma(D)$ also differ from their values at $D = \infty$ by terms which are exponentially small as a function of D.

The thermodynamic argument of §2 derives the Kelvin equation (7) for the shift in the transition temperature by balancing bulk and surface free energy terms. In the context of the present model this can be derived from the free energy expression of equation (40),

$$\phi = 2\sigma(D = \infty) + D/\xi F(\eta_b) + 2[\sigma(D) - \sigma(\infty)] + D/\xi[F(\eta_m) - F(\eta_b)]. \tag{47}$$

The asymptotic behaviour of Δt_{NI} as a function of D results from the first two terms in this expression; the last two terms are exponentially small and can be neglected. Thus in the asymptotic regime the normalized shift in the phase transition temperature Δt_{NP} is given by

$$\Delta t_{NP} = 2t_{NP}[\sigma_P(\infty) - \sigma_N(\infty)]\xi/Dl, \tag{48}$$

where σ_P, σ_N are the paranematic–wall and nematic–wall surface free energies respectively, $l = t_{NP}(s_P - s_N)$ is the (normalized) latent heat at the phase transition, and

$$s = -\frac{\partial F}{\partial t} \tag{49}$$

is the bulk entropy density, with the subscripts p and N applying to the paranematic and nematic phases respectively. Expression (48) is expected to be exact in the limit $D \to \infty$, but, as we shall see, this approximation can also be rather good for quite small D so long as the wall potential is not too strong. These observations have been made before in discussing phase transitions in finite systems [10, 11]; Evans *et al.* [12] drew attention to their connection with the thermodynamic results.

We have already emphasised in §2 the dependence of t_{NP} on the nematic–wall contact angle θ, and the particular significance of the cases $\theta = 0$ and $\theta = \pi$ when complete wetting by the nematic and paranematic phases occurs, respectively. We recall that in the one-wall case for $\theta = 0$ there can, under some circumstances, be a boundary layer transition at which η_0 (but not η_b) jumps. For finite D this transition persists, although now the large jump in η_0 is accompanied by an exponentially small jump in η_m with a functional form given by equation (46). Sheng [3] found that this line of boundary layer transitions is parallel to the D axis, essentially because of the exponentially small corrections to η_0 and $\eta_m \approx \eta_b$. For smaller D the boundary layer transition temperature would no longer be independent of D, but apparently the transition disappears at rather large thicknesses ($D/\xi \approx 100$) where the asymptotic relations still hold.

For paranematic wetting ($\theta = \pi$) the situation is analogous, although $\Delta t_{NP} < 0$. However, in the case of zero bulk magnetic field ($h = 0$) the conditions for complete wetting by the isotropic phase are rather restrictive; in particular $h_1 = 0$. The nature of the wetting phase diagram now prohibits a boundary layer transition [1].

The distinguishing feature of complete wetting in the semi-infinite system is that the surface structure shows no discontinuity at the phase transition. In particular, in the context of the present model, even though η_b jumps discontinuously at the phase transition, η_0 only undergoes a continuous transition at t_{NI}. This is no longer the case for a sample of finite thickness. A question of some theoretical interest is the functional form and magnitude of the jump $\Delta\eta_0(D)$ at the transition temperature $t_{NP}(D)$. To investigate this we first note that

$$F(\eta_m(D), t_{NP}(D)) \cong F(\eta_b, t_{NI}) - s_b \Delta t_{NP}, \tag{50}$$

$$F(\eta_0(D), t_{NP}(D)) \cong F(\eta_0, t_{NI}) - s_0 \Delta t_{NP}, \tag{51}$$

where $s_b(\eta_b)$ is the bulk entropy density, η_b corresponds to either the nematic or isotropic phases, and $s_0 = -\left.\dfrac{\partial F}{\partial t}\right|_{\eta_0, t_{NI}}$. Terms exponentially small in D have been neglected; they are small compared to $\Delta t_{NP} \sim D^{-1}$. We now combine equation (50) and (51) with the relation (32) to obtain

$$\begin{aligned} F_m(\eta_0^+, t_{NI}) - F_m(\eta_0^-, t_{NI}) &= [(s_0^+ - s_0^-) + (s_N - s_I)]\Delta t_{NP}, \\ &\sim D^{-1}, \end{aligned} \tag{52}$$

where

$$\eta_0^{\pm} = \eta_0(t_{NP}^{\pm}(D)).$$

In general we expect $\eta_0^+ \approx \eta_0^- \approx \eta_0(D = \infty)$; then from equation (32)

$$F_m(\eta_0^+) - F_m(\eta_0^-) \approx \left.\frac{\partial F_m}{\partial \eta_0}\right)_{\eta_0} \Delta\eta_0, \tag{53}$$

where $\Delta\eta_0 = \eta_0^+ - \eta_0^-$ and hence combining equations (52) and (53)

$$\Delta\eta_0 \sim D^{-1}. \tag{54}$$

This behaviour applies if the nematic phase wets the wall. However, if the isotropic phase wets the wall this reasoning does not apply. Now $\eta_0(D = \infty) = 0$, and as we have observed previously this only obtains when

$$V_s(\eta_0) = \tfrac{1}{2}g\eta_0^2. \tag{55}$$

We must still have $\eta_0^+ = 0$, although $\eta_0^- \neq 0$. In this case, using equation (32),

$$\frac{\partial F_m}{\partial \eta_0} = \frac{\partial F}{\partial \eta_0} - \tfrac{1}{2}V_s'(\eta_0)V_s''(\eta_0). \tag{56}$$

Now $\eta_0 = 0$ is itself a local solution of the bulk statistical mechanics, so $\partial F/\partial\eta_0 = 0$, and hence by combining equations (55) and (56), we have $\partial F_m/\partial\eta_0 = 0$. Thus in this case

$$F_m(\eta_0^+) - F_m(\eta_0^-) \simeq \frac{1}{2}\frac{\partial^2 F_m}{\partial \eta_0^2}\Delta\eta_0^2, \tag{57}$$

and combining equations (52) and (57) yields the asymptotic behaviour

$$\Delta\eta_0 \sim D^{-1/2}. \tag{58}$$

Finally in this section we discuss the behaviour of the average order parameter

$$\bar{\eta} = \frac{1}{D}\int_0^D \eta(z)dz = \pm\frac{2}{D}\int_{\eta_0}^{\eta_m}\frac{[\eta - \eta_m]\,d\eta}{\sqrt{[F(\eta) - F(\eta_m)]}} + \eta_m \tag{59}$$

close to the paranematic–nematic phase transition. This quantity is experimentally accessible in, for example, a birefringence experiment. Whereas in the bulk system η_b jumps from zero to η_N at t_{Ni} (for $h = 0$), in general in the finite D case $\bar{\eta}$ shows some pretransitional behaviour, and is non-zero (although relatively small) even above t_{NI}. The only exception to this is the case when the surface field h_1 is identically zero; as we have discussed, then and only then $\eta_0 = \eta_m = \bar{\eta} = 0$ everywhere above t_{NI}. We shall, for definiteness, study the behaviour of $\bar{\eta}(t_{NP}^+(D))$, the value of the average order parameter in the paranematic ('isotropic') phase just above the phase transition. We must deal with the two cases, complete wetting by the nematic phase, and partial wetting, separately. In both cases, however, because the corrections to η_0 and η_m are exponentially small, the leading behaviour for large D is given by

$$\bar{\eta} \cong \frac{2\Gamma}{D}, \tag{60}$$

where

$$\Gamma = \int_0^\infty (\eta(z) - \eta_b)\,dz$$

is the adsorption on a single wall in the semi-infinite system.

As discussed in §2, for complete wetting,

$$\Gamma(t) \sim \ln(t - t_{NI}), \tag{61}$$

from which $\Gamma(t_{NP}^+(D)) \sim \ln\Delta t_{NP} \sim \ln D$, and hence

$$\bar{\eta}(t_{NP}^+(D)) \sim \ln D/D. \tag{62}$$

On the other hand for partial wetting Γ remains finite at t_{NI}, and is an analytic function of t in this region. Thus

$$\Gamma(t_{NP}) \approx \Gamma(t_{NI}) + \Delta t_{NP}\left(\frac{\partial \Gamma}{\partial t}\right)_{t_{NI}} + \ldots, \tag{63}$$

and substituting from equation (63) into equation (60) we obtain

$$\bar{\eta}(t_{NP}^{+}(D)) \sim \frac{1}{D} + 0\left(\frac{1}{D}\right)^2. \tag{64}$$

There are analogous effects below the phase transition; the relevant quantity to study is $\bar{\eta}(t_{NP}^{-}(D)) - \eta_N(t_{NI})$. However these effects are much more difficult to measure.

6. The nematic–paranematic phase diagram

We first present the method for the calculation of the nematic–paranematic phase diagram, for $h = 0$, and the results of the calculations. The calculations themselves are by no means trivial, and we postpone a more complete description to Appendix 2, in which we also give some general arguments about the shape of $\eta(z)$ under various circumstances.

In general, the strategy used to determine the phase diagram is to plot $D(\eta_0)$ for a given temperature t. This graph, in general, has a number of branches, one of which is the thermodynamic branch. At the phase boundary the free energy corresponding to two different branches is the same. The phase boundary at $D = \infty$ is known. For very small D^{-1} the phase boundary can be plotted using the Kelvin equation (48). For higher D^{-1}, the Clausius–Clapeyron relation (17) must be used. In the context of the present model this equation becomes

$$\left(\frac{dt}{dD}\right)_{\Delta\phi=0} = -\frac{\left(\frac{\partial \Delta\phi}{\partial D}\right)_t}{\left(\frac{\partial \Delta\phi}{\partial t}\right)_D} = \frac{\Delta F_m}{D\Delta\bar{s}} = -\frac{2\xi\Delta\sigma}{D^2\Delta\bar{s}}, \tag{65}$$

where

$$\left(\frac{\partial \phi}{\partial t}\right)_D = \left(\frac{\partial \phi}{\partial t}\right)_{D,\eta_0,\eta_m} = -\bar{s}D/\xi = -\int_0^D s(z)\,\frac{dz}{\xi}, \tag{66}$$

and $s(z)$ is the local entropy density. Using D^{-1} as the independent variable we obtain

$$\frac{dt_{NP}}{dD^{-1}} = 2\xi\,\frac{(\sigma_P - \sigma_N)}{(\bar{s}_P - \bar{s}_N)}. \tag{67}$$

The average entropy $\bar{s}$ can be expressed in terms of η_0, η_m and D as

$$\bar{s} = s(\eta_m) - \frac{3}{2}\left(\frac{\xi}{D}\right)\left|\int_{\eta_0}^{\eta_m} \frac{\eta^2 - \eta_m^2}{F(\eta) - F(\eta_m)}\,d\eta\right|. \tag{68}$$

In principle the relation (67) is exact. In practice this relation is used to provide a guess for $t_{NP}(D)$, and knowledge of the functions $D(\eta_0)$ and $\phi(D, \eta_0)$ is then used to improve this guess.

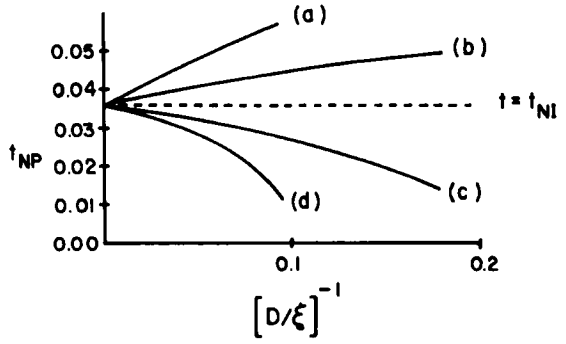

Figure 1. Phase boundaries in the (D^{-1}, t) plane. (*a*) $h_1 = 0{\cdot}02, g = 0$; (*b*) $h_1 = 0{\cdot}01, g = 0$; (*c*) $h_1 = 0{\cdot}01, g = 0{\cdot}15$; (*d*) $h_1 = 0{\cdot}02, g = 0{\cdot}4$.

We show in figure 1 the phase diagram in (t, D^{-1}) space for a number of different values of h_1 and g. Certain generic features of the phase diagram (the shift in coexistence curve and the existence of a critical point) are universal. Only when the wall is completely disordering ($h_1 = 0$), do we not find the existence of a critical point. Depending on the value of the contact angle $\cos\theta$, the phase transition temperature $t_{NP}(D)$ increases or decreases as a function of D^{-1}. The other dramatic feature which accompanies the shift in t_{NI} is a change in the behaviour of the mean order parameter $\bar{\eta}(t)$. We show in figure 2 schematic representations of the behaviour of $\bar{\eta}(t)$ as D^{-1} is increased, for a number of different cases. In figure 2 (*a*) we show the behaviour of $\bar{\eta}(T)$ for different D for strongly ordering walls. Roughly speaking this corresponds to the phase diagram of figure 1 (*a*) or (*b*). In figure 2 (*b*) we show the behaviour of $\bar{\eta}(T)$ for weakly ordering walls, for which $\cos\theta < 0$. This corresponds to the phase diagram 1 (*c*) or (*d*). In figure 2 (*c*) we show $\bar{\eta}(T)$ for disordering walls. In the first two cases there is a small amount of ordering above t_{NI}. In the last case there is no critical point.

In figure 1 the dependence $t_{NI}(D)$ is described by the Kelvin approximation $\Delta t_{NI} \sim D^{-1}$ in the asymptotic regime $D^{-1} \to 0$. For small values of h_1 and g this approximation is good in practice up to the critical point. We find that the Kelvin equation can only be satisfied for smaller separations if partial wetting conditions obtain. Figure 1 (*a*) with $h_1 = 0{\cdot}02, g = 0$ appears to give linear D^{-1} dependence for t_{NI}. However, its slope for larger D^{-1} differs from that predicted by the Kelvin equation. This phenomenon is connected to the boundary phase transition, which occurs ($g = 0$) for $0{\cdot}014 < h_1 < 0{\cdot}024$. For smaller values of D the modified transition temperature is sufficiently high that it pre-empts the boundary phase transition. The behaviour of $t_{NI}(D)$ is still governed by the asymptotic rule, but now the appropriate surface free energy to take is the metastable low η_0 value, rather than the stable high η_0 value. The low η_0 value is stabilized by the increase in t_{NI}. It corresponds to a higher value of σ_1 than the stable value (which is just $\sigma_N + \sigma_{NI}$), or equivalently, a value of $\cos\theta > 1$. Thus in figure 1 (*a*) we have the apparently anomalous example of a surface phenomenon governed by a value of $\cos\theta = (\sigma_1 - \sigma_N)/\sigma_{NI} > 1$.

At this point we remark on the strong analogy between the nematic phase diagram in a bulk system in a bulk magnetic field h, and the nematic phase diagram in a confined system as a function of the inverse wall spacing D^{-1}. This analogy was noticed by Sheng [3], and is implicit in the use of the term *paranematic* for the less ordered phase in both cases. However, unrealistically large bulk magnetic fields are

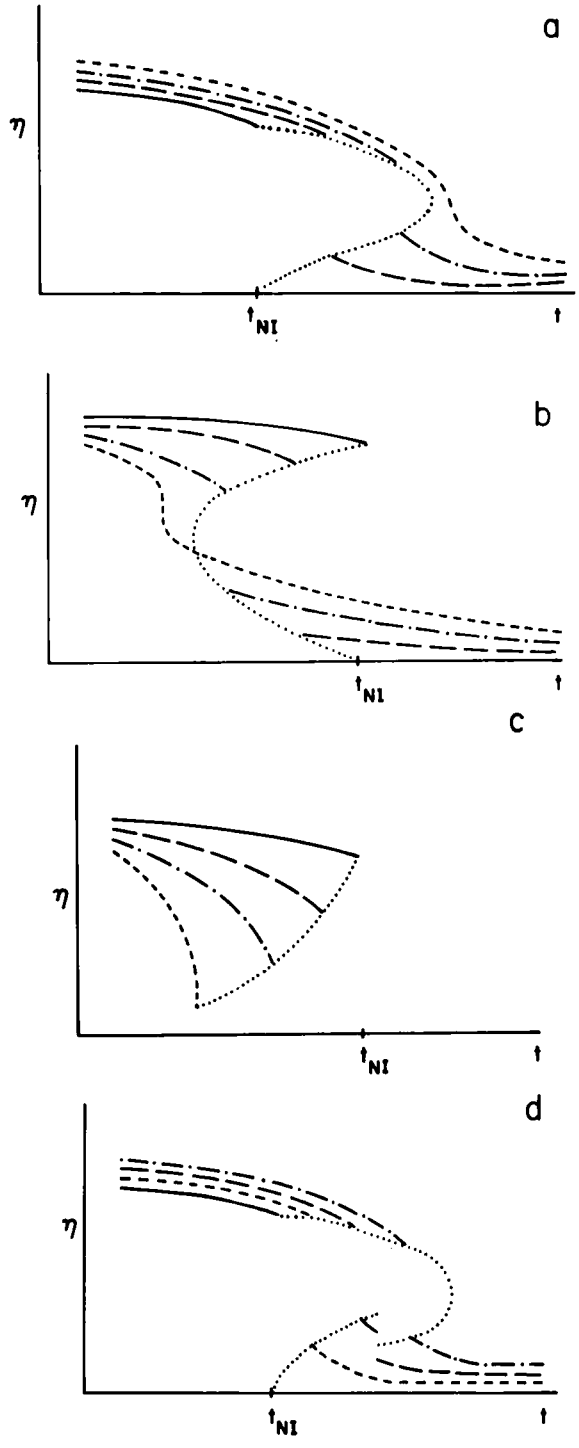

Figure 2. Schematic plots of the mean order parameter $\bar{\eta}$ against temperature t. (*a*) $\cos\theta > 0$; (*b*) $\cos\theta < 0$; (*c*) $g = 0$; purely disordering boundary. Curves 1 (——), 2 (— —), 3 (-·-·) and 4 (- - - - -) are in order of decreasing thickness. Curve 1 is $D = \infty$. (*d*) includes the boundary transition.

required to observe the bulk nematic–paranematic critical point. We therefore pose the question: is the analogy between these two phenomena more than just a formal analogy, so that by observing the finite geometry phenomena we may think of ourselves as observing the bulk nematic–paranematic phase diagram in another guise? We examine this question further in the next subsection.

6.1. *The critical point*

We make the simplest approximation, which is to suppress spatial variations of the order parameter, and suppose that surface fields can be averaged over the bulk. The liquid crystal is now treated as if it were in an effective external uniform ordering field

$$h_{\text{eff}}(\bar{\eta}) = 2V_s(\bar{\eta})/(D/\xi), \tag{69}$$

where $\bar{\eta}$ is a (suitably defined) average order parameter, and the free energy density is now given by equation (19)

$$\begin{aligned} F(\bar{\eta}) &= \tfrac{3}{4}t\bar{\eta}^2 - \tfrac{1}{4}\bar{\eta}^3 + \tfrac{9}{16}\bar{\eta}^4 + h_{\text{eff}}(\bar{\eta}), \\ &= \tfrac{3}{4}(t + \tfrac{4}{3}g\xi/D)\bar{\eta}^2 - \tfrac{1}{4}\bar{\eta}^3 + \tfrac{9}{16}\bar{\eta}^4 - 2h_1(\xi/D)\bar{\eta}. \end{aligned} \tag{70}$$

The net effect is not only to introduce an effective ordering field but also to shift the temperature scale downwards. The reduced number of surface nearest neighbours means that the temperature required for the onset of nematic behaviour is lowered.

The critical parameters can now be found by comparing the parameters in the free energy of equation (70) to those in equation (19). We obtain for the critical thickness,

$$2h_1(\xi/D_{\text{cr}}) = h_c, \tag{71}$$

and hence

$$D_{\text{cr}}/\xi = 2h_1/h_c; \tag{72}$$

for the critical temperature

$$t_{\text{cr}} + \tfrac{4}{3}g\xi/D_{\text{cr}} = t_c, \tag{73}$$

whence, combining equations (72) and (73) we obtain

$$t_{\text{cr}} = t_c - \tfrac{2}{3}g(h_c/h_1). \tag{74}$$

In figures 3, 4 and 5 we compare the predictions of equation (72) and (74) with those of the full non-uniform theory. In figure 3 a plot of D_{cr} against h_1 is shown for a number of different values of g/h_1. The predictions of equation (72) are remarkably well satisfied, especially for low h_1. Discrepancies occur for higher h_1, in particular for large values of g/h_1. Equation (74) predicts that $t_{\text{cr}} = t_{\text{cr}}(g/h_1)$, and for $h_1 \lesssim 0{\cdot}02$ this is very well satisfied. Equation (74) also predicts that if $h_1 = 0$, $t_{\text{cr}} \to -\infty$, or equivalently that no critical point exists, and this also is consistent with the predictions of the full theory. On the other hand if $g = 0$, equation (74) predicts that t_{cr} should be independent of h_1. In figure 4 we compare this approximation to the full theory. For low h_1 this is well-satisfied, although we find numerically a slight decrease in t_{cr}. Above $h_1 \sim 0{\cdot}02$ there is a more marked decrease in t_{cr}, which then stabilizes at a lower value of t_{cr} around $h_1 \sim 0{\cdot}03$ [20]. In figure 5 we check the prediction of equation (72) for the functional dependence of D_{cr} on h_1, for the case $g = 0$. Once again we notice that the prediction is well satisfied for $h_1 \lesssim 0{\cdot}02$, but there are significant deviations for higher h_1.

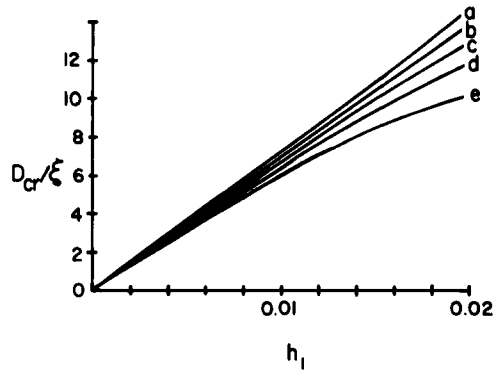

Figure 3. Comparison of the predictions for D_{cr} as a function of h_1 using the full non-uniform theory and a simple averaged field approximation. Line (*a*) corresponds to $g = 0$; line (*c*), $g/h_1 = 5$; line (*d*), $g/h_1 = 10$; line (*e*), $g/h_1 = 30$. Line (*b*) is the prediction of the averaged field approximation.

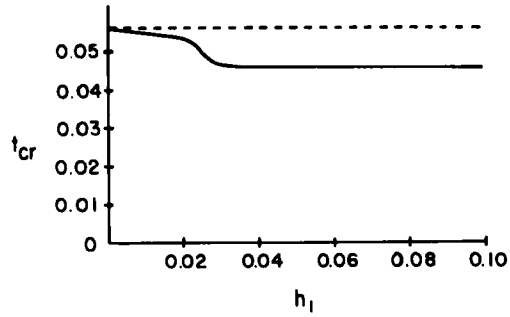

Figure 4. Prediction for t_{cr} as a function of h_1 for $g = 0$. The dotted line $t = t_c$ is the average field prediction.

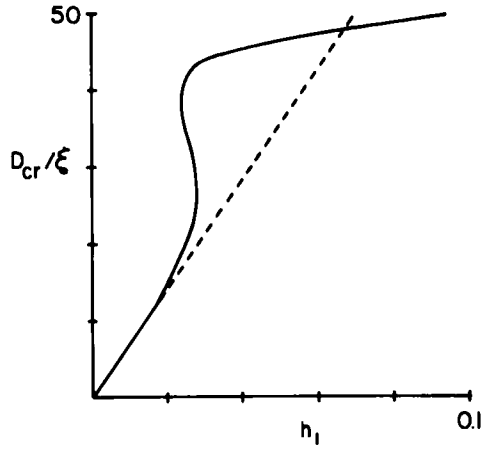

Figure 5. Prediction for D_{cr} as a function of h_1 for $g = 0$ in the large h_1 regime.

We now make some brief comments on these results. The simple theory approximates the full theory well, from the point of view of predicting the critical parameters, for $h_1 < 0{\cdot}02$. By comparison we remark that complete wetting by the nematic phase occurs at $h_1 = 0{\cdot}014$, and the last vestige of non-wetting behaviour, the surface critical

point, occurs at $h_1 = 0{\cdot}024$. It seems likely, therefore, that the approximate theory loses its validity at the onset of complete wetting. Why this should be is not clear. We speculate that this might be because the finite thickness system has two nematic–isotropic interfaces which in some sense screen the effect of the surface field from the centre of the sample, thus lowering the critical temperature. We observe that at very high fields the critical temperature seems to stabilize, but at a lower temperature from that predicted by the simple theory. We do not understand this phenomenon, although it seems likely that there is a simple qualitative explanation. This is, however, precisely the regime in which the Kelvin equation also needs corrections as a result of the growth of nematic layers close to the wall.

6.2. *Comparison with experiment*

Yokoyama *et al.* [7] carried out experiments on liquid crystal 4-*n*-pentyl-4′-cyanobiphenyl (5CB) between SiO and PVA substrates. Essentially the experiment measures $\bar{\eta}(T)$. A quantitative comparison between experiment and theory is rather difficult at this stage mainly because the experimental data do not provide a precise determination of the critical thickness and temperature. Nevertheless we have been able to estimate values for the surface parameters h_1 and g using the approximate formulae (72) and (74). If for the SiO surfaces we estimate $D_{cr} \approx 1100\,\text{Å}$ and $T_{cr} - T_{NI} = -0{\cdot}1\,\text{K}$, then we find $h_1 = 0{\cdot}129$ and $g = 1{\cdot}38$. In physical units this leads to $h_1 \sim 0{\cdot}53 \times 10^{-3}\,\text{J m}^{-2}$ and $g = 0{\cdot}57 \times 10^{-2}\,\text{J m}^{-2}$. For the PVA surfaces if we estimate $D_{cr} \cong 1600\,\text{Å}$ and $T_{cr} - T_{NI} = 0{\cdot}03\,\text{K}$, this leads to $h_1 = 0{\cdot}187$ and $g = 1{\cdot}6$, corresponding to physical values of $h_1 \sim 0{\cdot}77 \times 10^{-3}\,\text{J m}^{-2}$ and $g \sim 0{\cdot}66 \times 10^{-2}\,\text{J m}^{-2}$. In both cases we have used for A, B, C and L values given by Sheng [21], and the matching between model and physical parameters is as described in equation (18) and (19). We notice, however, that the energy scale seems rather large compared to the nematic–isotropic surface tension in 5CB of $\sim 2 \times 10^{-5}\,\text{J m}^{-2}$; further work would appear to be fruitful.

7. Structural forces in nematic films

We now turn to the structural force between the two walls, which as shown in §4, is given by

$$\pi_D = -[F(\eta_m) - F(\eta_b)]. \tag{75}$$

The condition (44) shows that π_D is an increasing function of D, and is zero at $D = \infty$. Hence in this model π_D is always negative, or equivalently the plates attract each other.

We can also analyse the asymptotic behaviour in the large D limit. Because $F'(\eta_b) = 0$,

$$F(\eta_m) - F(\eta_b) \sim (\eta_m - \eta_b)^2, \tag{76}$$

and from equation (46), we expect

$$\pi_D \sim \exp\{[-\tfrac{1}{2}F''(\eta_b)]^{1/2} D/\xi\}. \tag{77}$$

This exponential behaviour is a characteristic of the contact short-range potential assumed for the surface forces. Power law surface forces would give rise to a power law dependence of π_D upon D [22].

The nematic–paranematic transition can be thought of as taking place at constant t_{NI} by allowing D to vary. The disjoining pressure goes through a discontinuity at the

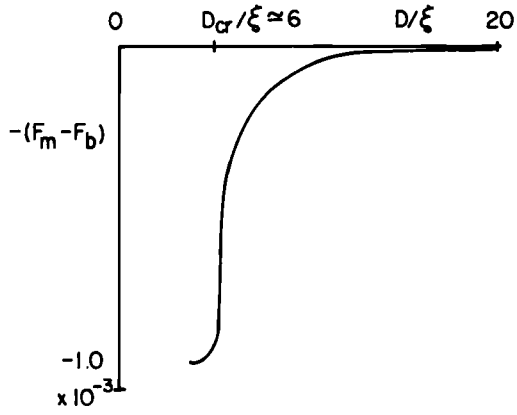

Figure 6. Disjoining force in the case $g = 0{\cdot}15$, $h = 0{\cdot}01$ at $t = 0{\cdot}2$ just below $t_{cr} = 0{\cdot}0247$.

transition. If $\Delta t = t_{NP}(D) - t_{NI} > 0$ the high D phase is paranematic, but if $\Delta t < 0$ the high D phase is nematic. In both cases, however,

$$\pi_D(D^-) < \pi_D(D^+) \tag{78}$$

and $\pi_D(D)$ remains an increasing function of D. The attractive disjoining forces violate the mechanical stability condition (44); they could not be observed in a simple experimental context [15].

The discontinuity $\Delta\pi_D = \pi_D(D^+) - \pi_D(D^-)$ along the coexistence line in (D^{-1}, t) space presents an interesting feature. In the asymptotic regime

$$\Delta\pi_D \sim \Delta F(\eta_m, t_{NP}(D)), \tag{79}$$

and hence from equation (50)

$$\Delta\pi_D \sim (s_I - s_N)\Delta t_{NP} \sim D^{-1}. \tag{80}$$

Thus initially $\Delta\pi_D$ increases as D^{-1} increases. However, as D is further reduced the discontinuity goes through a maximum and decreases, finally disappearing at the critical point.

In figure 6 we present a typical plot of π_D against D, at constant t. We have chosen $h_1 = 0{\cdot}01$ and $g = 0{\cdot}15$, the phase diagram of which is given in figure 1 (*c*); for these parameters $t_{cr} = 0{\cdot}0247$ and $D_{cr}/\xi \approx 6$. The plot is at $t = 0{\cdot}02 < t_{cr}$. The significant features are the high D exponential behaviour, the rapid rise in π_D close to D_{cr}, and the lower $d\pi_D/dD$ for smaller D. The large $d\pi_D/dD$ in the region of D_{cr} is a critical effect indicating the closeness of the critical point; at the critical point this quantity diverges.

We would like to make contact with the experiment carried out by Horn *et al.* [15]. They measured the force between mica surfaces separated by the nematic liquid crystal 5CB in both planar and homeotropic orientations at room temperature. They found repulsive medium range structural forces and speculated that the modification of the order parameter near the surfaces was responsible for these forces. The repulsive structural forces cannot therefore be explained by the present model, confirming a prediction by Marčelja and Radić [23] who made an incomplete calculation using a simpler version of our model. In fact the experiment of Horn *et al.* was slightly more complicated than two parallel plates; in their experiment a drop of liquid crystal was placed between two cylindrical surfaces whose symmetry axes were parallel. However, this cannot change the qualitative picture. The attractive nature of the structural

forces should be independent of the detailed form of $V_s(\eta)$, so long as it is assumed to be a contact potential. If $V_s(\eta)$ had non-zero range this might make a difference. Repulsive structural forces have been predicted at short range [24], but these are due to intermolecular correlations, and the range is much shorter than the experimental range. Evans *et al.* [12] studied the statistical mechanics of thin liquid films using a non-local density functional approach. In this system it is the density rather than the orientational order which changes, but otherwise there are strong analogies with the system we study.

However, if the primary ordering force at the surfaces is dipolar, and only indirectly nematic through the coupling between polar and nematic order parameters, then repulsion between the walls is possible, as we now show. We write the free energy per unit volume as a function of a polar order parameter p, and ignore its dependence on the nematic order parameter η:

$$F(p) + \zeta^2\left(\frac{dp}{dz}\right)^2 = \bar{F} + \tfrac{1}{2}ap^2 + \cdots + \zeta^2\left(\frac{dp}{dz}\right)^2, \tag{81}$$

where F is in general an even function of p, $a > 0$ implies that there is no spontaneous dipolar order, and for simplicity we take $F(p)$ to have the simple form as in equation (81). We have introduced a dipolar correlation length ζ. The polar order parameter p is in general a vector, but if the walls force p to be in the z direction, we take $p = p_z$ to be a scalar. We shall not specify a particular form of the surface field $V_s(p)$, other than to observe that if the walls are identical,

$$p_s = p(0) = -p(D), \tag{82}$$

and $p(z)$ is *antisymmetric* about $z = D/2$, by contrast with $\eta(z)$ which is symmetric, and consequently $p(D/2) = 0$. The Euler–Lagrange equations for p and the crucial thermodynamic quantities can be written down by analogy with equations (27), (28), (40), (41), the equivalent equations for η; we find

$$\zeta^2\left(\frac{dp}{dz}\right)^2 = F(p) - F(0) + K_m^2 = F(p) - F_m, \tag{83}$$

where

$$K_m = \zeta\left(\frac{dp}{dz}\right)_{z=D/2}, \tag{84}$$

$$\phi = 2\sigma + (D/\zeta)F_m, \tag{85}$$

and the disjoining force is given by

$$\pi_d = -(F_m - F_b), \tag{86}$$

where the bulk free energy density F_b is

$$F_b = F(0). \tag{87}$$

Combining equations (83), (86) and (87) we obtain immediately

$$\pi_D = K_m^2 > 0, \tag{88}$$

or equivalently a *repulsive* long-range force between the plates. The large D behaviour of the disjoining force can be obtained from the analogue of equation (31),

$$\frac{D}{\zeta} \cong \int_0^{p_s} \frac{dp}{\sqrt{(\frac{1}{2}ap^2 + K_m^2)}}, \tag{89}$$

from which, combining equations (88) and (89),

$$\pi_D \sim \exp[-\tfrac{1}{2}(\tfrac{1}{2}a)^{1/2}D/\zeta]. \tag{90}$$

In fact we expect both dipolar and nematic effects at the interfaces, which give rise to competing attractive and repulsive forces. A further complication might be the long-range nature of the electrostatic forces which interact with the dipoles. The crucial feature which ensures the repulsive force, however, is the anti-symmetry of the profile $p(z)$ around the centre of the slab. The experimentally observed repulsive disjoining force is thus indirect evidence of the importance of surface dipolar forces, giving rise to surface dipole order. The dipolar forces do not need to be strictly electrical dipole forces; there is no evidence to suggest that mica is electrically active. However the molecules of 5CB do not have complete inversion symmetry along their major axis, and this may give rise to surface forces leading to dipolar surface order. We emphasize however that surface nematic order alone leads to an attractive disjoining force.

8. Conclusions

The primary aim of this study has been the investigation of the statistical mechanics of a directionally uniform nematic, in a thin slab between identical walls, in particular close to the nematic–isotropic transition. We have used a Landau–de Gennes mean field type theory with surface interactions of zero range. The theory is a one order parameter theory, and as such is applicable close to any order–disorder transition in a thin slab geometry. A secondary aim of this study has been to make a general contribution to the theory of the effects of finite size on first order phase transitions. We have also endeavoured, as some previous workers have not, to maintain contact between the results of the statistical mechanical calculations and more general thermodynamic considerations.

The theory predicts, almost universally, that in a finite slab the first order nematic–isotropic transition is shifted, and for sufficiently thin systems this first order line terminates at a critical point. For large thicknesses the shift in transition temperature is inversely proportional to thickness, as predicted by the thermodynamic Kelvin approximation. For thinner systems the coexistence line is described by a Clausius–Clapeyron relation. In fact in many cases the asymptotic, large thickness result remains true even at lower thicknesses. The only exception, within the theory, to the generic phase diagram occurs when the walls are completely disordering; then there is no critical point. So long as this is not the case the high temperature isotropic phase is properly called a paranematic phase, because of the wall-induced order. This order can become quite significant close to the transition, in particular when the walls are wet by the nematic phase, and as the critical point is approached.

For many cases of partial wetting ($\cos\theta \neq 0$ or π) the walls are such as to slightly favour order when the bulk phase is disordered, but to disfavour order when the bulk is nematic. In the thick slab there will then be two possible shape profiles, one with increased and the other with decreased wall order. Although the nematic and paranematic profiles become identical at the critical point, in general the shape of the profile changes before the critical point, and depends on whether $V_s'(\bar{\eta})$ is greater than or less than zero.

The statistical mechanics of the finite thickness system has a strong analogy with that of a nematic in an ordering field. Indeed, our results show that in the weak surface

field regime the phase diagram of the finite system would be well predicted by averaging the surface fields over the whole system. The finite magnetic field critical point has not hitherto been experimentally accessible; the finite thickness effects are perhaps more so.

We have also studied the structural force between two walls. We find that surface nematic ordering gives rise to attractive forces between walls, but that the experimentally observed repulsion can only be understood in terms of surface dipole ordering.

The calculations of the asymptotic behaviour of various parameters in the large D limit should be directly amenable to experiment. We draw particular attention to behaviour of the discontinuity in the surface order parameter ($\Delta\eta_0$ in §5) when the wall is such that one phase (either N or I) completely wets it. We find that in the large D limit, this discontinuity is normally inversely proportional to thickness (recalling that in a semi-infinite system it would be continuous). However the discontinuity is proportional to $D^{-1/2}$ if the parameters at the wall are appropriate to a critical wetting transition. This includes the particular case of a wall wet by the isotropic phase. Such wetting is in a sense less powerful, and unsurprisingly $\Delta\eta_0$ is greater, i.e. $D^{-1/2} > D^{-1}$. Finally, of course, if the wall is not completely wet by either phase $\Delta\eta_0$ remains finite at $D^{-1} = 0$, which is larger still.

We next ask in what way the modelling of the problem might be incomplete. The contact interactions at the wall are an approximation which will give rise to incorrect asymptotic behaviour of the disjoining pressure at large thicknesses. If the surface interactions are power-law like this could be serious; however liquid crystal orienting interactions may be short-range. In any event the experiments remain unexplained and further experiments are clearly desirable. Similar qualifications apply to the whole Landau–de Gennes formalism, but it has proved useful in other contexts.

Perhaps a larger problem is concerned with the effect of fluctuations. For the nematic–isotropic transition fluctuations are important even for bulk three-dimensional systems, in the sense that the Ginzburg criterion [25] is not satisfied close to the transition. Presumably this becomes even more important for a thin system which is becoming in some sense two dimensional. This may mean that the theory is unreliable from a quantitative point of view, especially for thinner slabs. However, presumably the qualitative picture remains viable. We note, however, that in a system of cylindrical or spherical pores, the fluctuations become sufficiently powerful to broaden the singularities associated with a first order phase transition. A mean field theory of the type used in this paper would be unable to treat this phenomenon. In the nematic case for such a geometry it would also no longer be possible to ignore director inhomogeneities.

Finally, we turn to directions for future research. First of all there is a need for further experiments. The experiments on the nematic–isotropic transition at finite thickness by Yokoyama *et al.* [7], while strongly suggestive, are by no means conclusive, and unambiguous observations of the finite thickness critical point are clearly desirable. Similarly there is a need for further experimental work on the disjoining pressure, especially in view of the possible competition between attractive and repulsive structural forces. On the theoretical side we emphasise that the present theory is in fact the simplest possible. More sophisticated attempts at modelling should include explicitly the possibility of density change close to walls and the full nematic ordering tensor. Intriguing phenomena may also result when the two walls are no longer identical, including the possibility that the ordering temperature may no longer be a monotonic function of thickness.

We thank members of the Liquid Crystal and Condensed Matter Theory Groups at Southampton University for providing us with a continuing stimulating intellectual environment. In particular we thank J. T. Chalker for reading an earlier version of the manuscript. Part of this work was carried out while A. P. was visiting Southampton University Chemistry Department, during which time he was supported by a grant from SERC (U.K.). He thanks G. R. Luckhurst for his hospitality. Some of the work was carried out during a visit by T. J. S. to the Institute of Physical Chemistry, Polish Academy of Sciences, Warsaw. He thanks the Polish Academy of Sciences and the British Council for financial support and J. Stecki for his hospitality.

Appendix 1

Derivation of the stability conditions

In this appendix we derive the stability conditions equations (38) and (39) used in the derivation of the equilibrium values of η_0 and η_m in §4. We recall that these quantities are solutions of the equations $\phi_{\eta_0} = 0$, $\phi_{\eta_m} = 0$ where $\phi(\eta_0, \eta_m)$ is described by equations (28) and (29). The stability equations, conditions that a minimum in ϕ has been found, are

$$\phi_{\eta_0\eta_0} > 0, \tag{A 1}$$

$$\phi_{\eta_0\eta_0}\phi_{\eta_m\eta_m} - \phi^2_{\eta_0\eta_m} > 0. \tag{A 2}$$

In fact the equation $\phi_{\eta_m} = 0$ yields an implicit relation between η_0, η_m and D, and as a result equation (A 2) can be rephrased as

$$\frac{d^2\phi}{d\eta_m^2} > 0, \tag{A 3}$$

where ϕ is now thought of as being a function of the one variable η_m.

From equation (28) we derive

$$\phi_{\eta_0\eta_0} = 2\sigma_{\eta_0\eta_0}. \tag{A 4}$$

Now from equation (29)

$$\sigma_{\eta_0} = \mp 2\sqrt{[F(\eta_0) - F(\eta_m)]} + V_s'(\eta_0), \tag{A 5a}$$

$$= 0. \tag{A 5b}$$

Hence

$$\sigma_{\eta_0\eta_0} = \mp \frac{F_{\eta_0}(\eta_0)}{\sqrt{[F(\eta_0) - F(\eta_m)]}} + V_s''(\eta_0). \tag{A 6}$$

We now substitute from equation (A 5) into equation (A 6), yielding

$$\sigma_{\eta_0\eta_0} = -\frac{2F_{\eta_0}(\eta_0)}{V_s'(\eta_0)} + V_s''(\eta_0), \tag{A 7}$$

$$= -\frac{2}{V_s'(\eta_0)}[F_{\eta_0}(\eta_0) - \tfrac{1}{2}V_s'(\eta_0)V_s''(\eta_0)], \tag{A 8}$$

$$= -\frac{2}{V_s'(\eta_0)}\frac{\partial}{\partial\eta_0}[F(\eta_0) - \tfrac{1}{4}(V_s'(\eta_0))^2], \tag{A 9}$$

and hence from equation (32)

$$\phi_{\eta_0\eta_0} = 2\sigma_{\eta_0\eta_0} = -\frac{4F_m'(\eta_0)}{V_s'(\eta_0)}. \tag{A 10}$$

Hence from equations (A 1) and (A 10) we derive the condition (38)

$$\frac{F_m'(\eta_0)}{V_s'(\eta_0)} < 0.$$

We shall derive equation (39) by starting with the condition (A 3). From equation (28)

$$\frac{d\phi}{d\eta_m} = 2\frac{d\sigma}{d\eta_m} + \frac{D}{\xi}\frac{dF(\eta_m)}{d\eta_m}, \tag{A 11 a}$$

$$= 0, \tag{A 11 b}$$

where equation (A 11 b) is the stationary condition, but can be thought of as the defining equation for a (locally defined) function $D(\eta_m)$. Then

$$\frac{d^2\phi}{d\eta_m^2} = 2\frac{d^2\sigma}{d\eta_m^2} + \frac{D}{\xi}\frac{d^2F(\eta_m)}{d\eta_m^2}. \tag{A 12}$$

However, using equation (A 11 b)

$$2\frac{d^2\sigma}{d\eta_m^2} = -\frac{d}{d\eta_m}\left[D(\eta_m)\frac{dF(\eta_m)}{d\eta_m}\right], \tag{A 13}$$

$$= -\frac{dD(\eta_m)}{d\eta_m}\frac{dF(\eta_m)}{d\eta_m} - D(\eta_m)\frac{d^2F(\eta_m)}{d\eta_m^2}, \tag{A 14}$$

and combining equations (A 12) and (A 14) we obtain

$$\frac{d^2\phi}{d\eta_m^2} = \frac{1}{\xi}[D - D(\eta_m)]\frac{d^2F(\eta_m)}{d\eta_m^2} - \frac{1}{\xi}\frac{dD}{d\eta_m}\frac{dF(\eta_m)}{d\eta_m}, \tag{A 15}$$

$$= -\frac{1}{\xi}\frac{dD}{d\eta_m}\frac{dF(\eta_m)}{d\eta_m}, \tag{A 16}$$

$$= -\frac{1}{\xi}\left[\frac{dF(\eta_m)}{d\eta_m}\right]^2\frac{dD}{d\eta_m}\Big/\frac{dF(\eta_m)}{d\eta_m}. \tag{A 17}$$

Now, recalling equation (32) $F_m(\eta_0) = F(\eta_m)$, and changing the independent variable from η_m to η_0, we derive

$$\frac{d^2\phi}{d\eta_m^2} = -\frac{1}{\xi}\left[\frac{dF(\eta_m)}{d\eta_m}\right]^2\frac{D'(\eta_0)}{F_m'(\eta_0)}. \tag{A 18}$$

Hence $\dfrac{d^2\phi}{d\eta_m^2} > 0$ implies the relation (39)

$$\frac{D'(\eta_0)}{F_m'(\eta_0)} < 0.$$

Appendix 2

In this appendix we discuss in more detail the behaviour of the graph of $D(\eta_0)$, derived from equations (31) and (32) and used in order to derive the phase diagram

discussed in §6. This will enable us to see more clearly the origin of the critical point within the theory, and we shall also see the connection between the graph of $D(\eta_0)$ and the shape of the profile $\eta(z)$.

We consider first the simplest case of $g = 0$; in this case the wall always orders the liquid crystal, so $\eta_0 > \eta_m$. We also find $\cos\theta > 0$ in the semi-infinite system, and from the Kelvin approximation $t_{NP}(D)$ increases as D decreases in the asymptotic large D regime, a trend which in fact continues for smaller D right up to the critical point. In figure 7 $D(\eta_0)$ has been plotted for an increasing sequence of temperatures, starting at t_{NI} and terminating at the nematic–paranematic critical temperature $t_{cr} = t_{NP}(D_{cr})$.

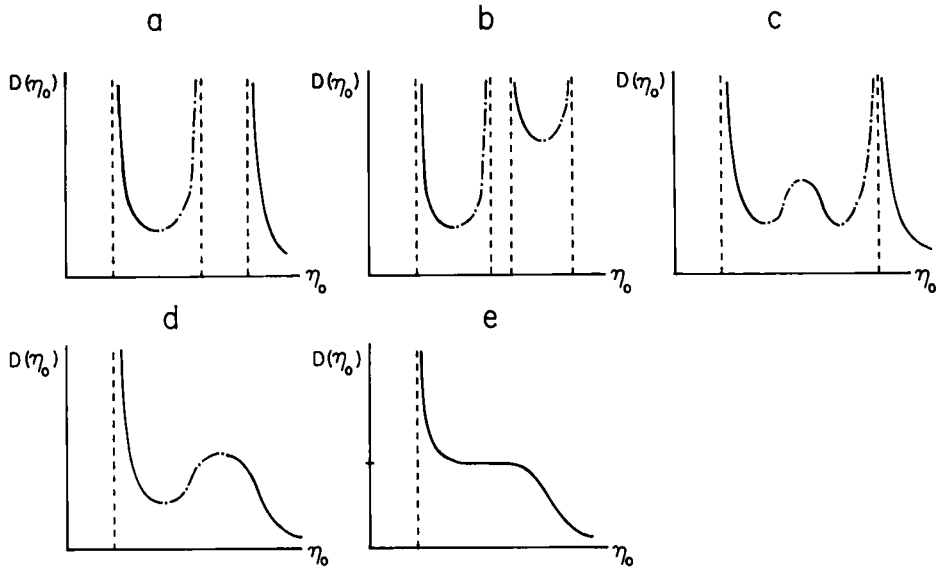

Figure 7. Graphs of $D(\eta_0)$ as temperature is increased for $g = 0$. (*a*) $t = t_{NI}$; (*b*) $t_1 > t_{NI}$; (*c*) $t_2 > t_1$; (*d*) $t_3 > t_2$; (*e*) $t = t_{cr}$.

The main features of these graphs can be understood as follows. For pedagogical reasons we start with figure 7 (*b*), in which $D(\eta_0)$ has three separate branches. The low η_0 solution corresponds to the thin film of low adsorption regime, i.e. low η_0 and low $\eta_m = \eta_b$ in the $D = \infty$ limit; the intermediate η_0 solution corresponds to the semi-infinite case in which the surface is more or less nematic, but the bulk is isotropic (the so-called thick or wetting film solution, η_m, is still small); the high η_0 solution corresponds to the nematic liquid. In all cases the physical solutions correspond to $D(\eta_0)$ being a decreasing function of D', this means that the smaller the system, the more the order, as expected for $h_1 > 0$. The regions where $D(\eta_0)$ is an increasing function of η_0 (the dotted lines) are unstable solutions. For $h_1 \lesssim 0{\cdot}12$ the nematic phase does not wet the wall and in general, the low η_0 branch is more stable than the intermediate branch. However for $h_1 > 0{\cdot}12$ we do get wetting and the intermediate branch is more stable. As discussed in equation (54) at the finite D transition to the nematic branch $\Delta\eta_0 \sim D^{-1} \sim \Delta t_{NP}$, indeed as t approaches t_{NI}, the wetting film solution for $D = \infty$ approaches the nematic solution; this corresponds to the

intermediate branch of $D(\eta_0)$ narrowing and squeezing towards the upper nematic branch of $D(\eta_0)$, as can be seen in figure 7 (*a*) where it has finally disappeared. On the other hand as t is increased the wetting film branch becomes progressively less stable and it disappears between figures 7 (*b*) and (*c*) for $D = \infty$, as the unstable thin film $D(\eta_0)$ branch hits the stable thick film branch. Thenceforth (figure 7 (*c*)) the thick film only leaves a ghost at finite D, in the form of an intermediate maximum of $D(\eta_0)$. Eventually the bulk nematic phase becomes unstable at a temperature $t_N^* (= \frac{1}{24}$ in our model for $h = 0$), and then only one branch of $D(\eta_0)$ remains (cf. figure 7 (*d*)). Notice however that a nematic phase still exists for low D, and the $D = \infty$ solution has now become a maximum in $D(\eta_0)$. Finally in figure 7 (*e*) at $t = t_{cr}$, $D(\eta_0)$ becomes monotonic with an inflexion point at $\eta_0 = \eta_0^{cr}$. The phase transition between the low η_0 and high η_0 branches of $D(\eta_0)$ disappears here, so this is the critical point.

The situation is slightly different for $h_1 \gtrsim 0{\cdot}024$, for then there is no boundary transition and only one possible value of η_0 for $D = \infty$, implying the absence of the left-hand branch in figures 7 (*a*) and (*b*). Figure 7 (*b*) is thus directly followed by figure 7 (*d*). Otherwise the picture is qualitatively the same. In all these cases the low temperature solution is the nematic branch. If t is increased at fixed D the solution jumps to another branch at a phase transition temperature $t_{NP}(D) > t_{NI}$. For $D \leqslant D_{cr}$, on the other hand, this is no longer possible and there is no phase transition.

We now examine what happens as we turn on progressively a surface disordering effect. The crucial quantity to monitor is η_0^*, defined by

$$V_s'(\eta_0^*) = -h_1 + g_1\eta_0^* = 0. \tag{B 1}$$

The two points to bear in mind, from equations (26) and (27), are that the sign of $V_s'(\eta_0)$ gives the sign of $(d\eta/dz)_{z=0}$, and that $(d\eta/dz)$ is monotonic for $0 < z < D/z$. From this we conclude that if $\eta_m > \eta_0^*$, then $\eta_m > \eta_0 > \eta_0^*$, and conversely if $\eta_m < \eta_0^*$ then $\eta_m < \eta_0 < \eta_0^*$. There are now three cases, depending on the size of η_0^*. We list and discuss them in order of increasing surface disorder, or equivalently, decreasing η_0^*.

In case (i) $\eta_0^* > \eta_N(t_{NI}) = \frac{2}{9}$. Then because $\eta_N(t)$ is a decreasing function of t, the surface potential is *ordering* both in the nematic phase and in the isotropic phase in the region of t_{NI}. The structure of $D(\eta_0)$ is now very similar to that in figure 7, and $t_{NP}(D) > t_{NI}$ as in that case also. There is one slight difference. Because $\eta_0 > \eta_m$, but also $\eta_0 < \eta_0^*$ in order to maintain the monotonicity of $\eta(z)$, as $D \to 0$, $\eta_0 \to \eta_0^*$. Because of the similarity of this case to the simple ordering case we do not show a separate diagram for this.

In case (ii) $\eta_0^* < \eta_N(t_{NI})$, but $\cos\theta > 0$. In this model $\cos\theta = 0$ corresponds to $h_1 = g\eta_c = g/9$ [1]. A metastable bulk nematic continues above t_{NI} with $\eta_N(t)$ decreasing with t, until it reaches bulk instability at $t_N^* (= \frac{1}{24}$ for $h = 0$ in this model), by which point η_N has reached η_N^*; in this model $F(\eta)$ has an inflexion point at $\eta_N^* = \frac{1}{6}$. The crucial region of interest is above t_{NI}, because $t_{NP}(D) > t_{NI}$. We consider case (ii (*a*)): $\eta_N(t_{NI}) > \eta_0^* > \eta_N^*$, and case (ii (*b*)): $\eta_N^* > \eta_0^* > \eta_c$ separately. In both cases, however, we observe that at t_{NI}, $V_s'(0) < 0$ in the isotropic phase and so as far as the isotropic phase is concerned the surface *orders*, but $V_s'(\eta_N(t_{NI})) > 0$, and hence from the point of view of the nematic phase the surface is *disordering*.

In figure 8 we show a number of plots of $D(\eta_0)$ for increasing values of t in case (ii (*a*)). In figure 8 (*a*), close to t_{NI}, there are two branches of $D(\eta_0)$. The left-hand branch is the isotropic branch. The physical part of this branch has D decreasing with η_0, corresponding to increased order at the surfaces. The right-hand branch is the

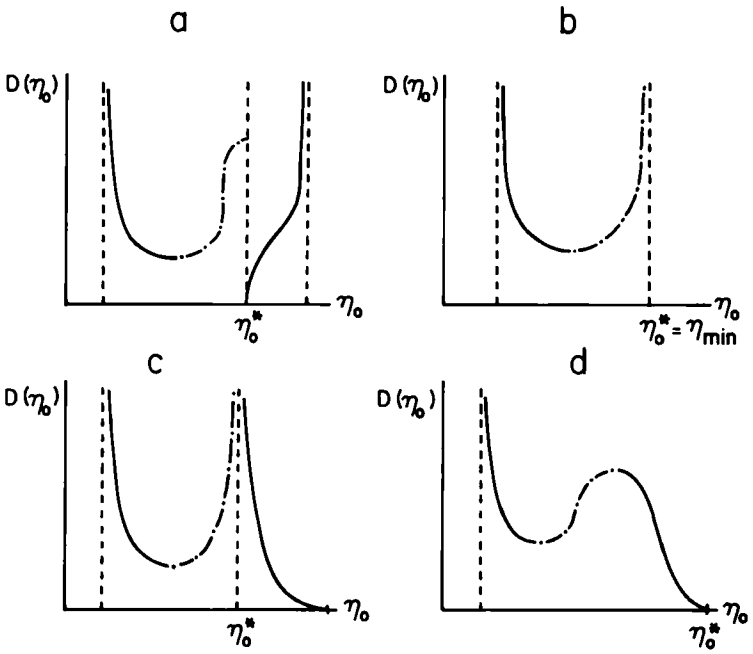

Figure 8. Graphs of $D(\eta_0)$ for $\cos\theta > 0$, $g \neq 0$; case (ii(*a*)) in the text. (*a*) $t = t_{Ni}$; (*b*) $t = t_1^* > t_{NI}$; (*c*) $t_1^* < t < t_N^*$; (*d*) $t_N^* < t < t_{cr}$.

nematic branch, but on this branch as η_0 decreases, so does D, corresponding to disordering surfaces. On this branch as $\eta_0 \to \eta_N^{*-}$, $D \to 0$. There is also an unstable $\eta_0 = \eta_0^*$ (for all D) branch, as can be seen from equations (26) and (27). The unstable part of the isotropic branch also hits $\eta_0 = \eta_0^*$, and terminates there, at a finite value of D, because the change of sign of $(d\eta/dz)$ at $\eta_0 = \eta_0^*$ destroys the solution. However as t increases $\eta_N(t)$ decreases, eventually reaching η_0^* in figure 8 (*b*). The surface is now *neutral* with respect to the nematic phase, and *ordering* with respect to the isotropic phase. The right-hand branch of $D(\eta_0)$ is thus squashed into the line $\eta_0 = \eta_0^*$. As t is further increased the nematic branch has D increasing with decreasing η_0, consistent with $\eta_N(t) < \eta_0^*$ and *ordering* interfaces (cf. figure 8 (*c*)). Note that $D(\eta_0^*)$ remains zero. The progression from figure 7 (*c*) to 8 (*d*) is analogous to that from figure 7 (*b*) to (*d*) in the case of continuous wetting: the bulk nematic is destabilized. Finally (not shown) a critical point is reached, by analogy with figure 7 (*e*).

Schematic order parameter profiles for the coexisting phases within the slab for case (ii (*a*)) are shown in figure 9. In figure 9 (*a*) the paranematic phase is more ordered near the walls, but the nematic phase is less ordered near the walls, corresponding to the respective branches of $D(\eta_0)$ in figure 8 (*a*). In figure 9 (*b*) the paranematic phase remains more ordered near the wall, but the nematic profile is constant, corresponding to $D(\eta_0^*)$ in figure 8 (*b*). However in figure 9 (*c*) both profiles are more ordered close to the wall, corresponding to subsequent pictures in figure 8, and remaining true at the critical point.

In figure 10 we present plots of $D(\eta_0)$ for case (ii (*b*)), for temperatures increasing from t_{NI} to $t_{cr}(D)$. Figure 10 (*a*) represents the situation at (and just above) t_{NI} and is analogous to figure 8 (*a*). We remark that in this figure the turning point of $D(\eta_0)$ takes place for $\eta_{max} < \eta_0 < \eta_0^*$, where η_{max} is the point at which $F(\eta)$ has a maximum. This can be seen from equation (32), which shows that $F(\eta_m)$ and η_m have turning points

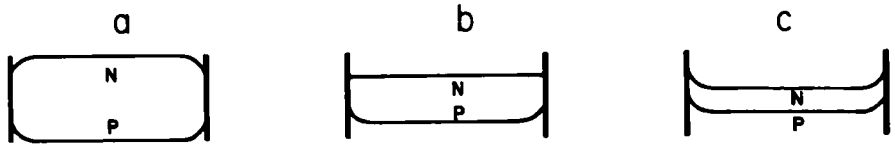

Figure 9. Coexisting profiles for the case described in figure 8. N is the nematic profile; P is the paranematic profile. (*a*) $t < t_1^*$; (*b*) $t = t_1^*$; (*c*) $t > t_1^*$. At $t = t_{cr} > t_1^*$ the two profiles become identical.

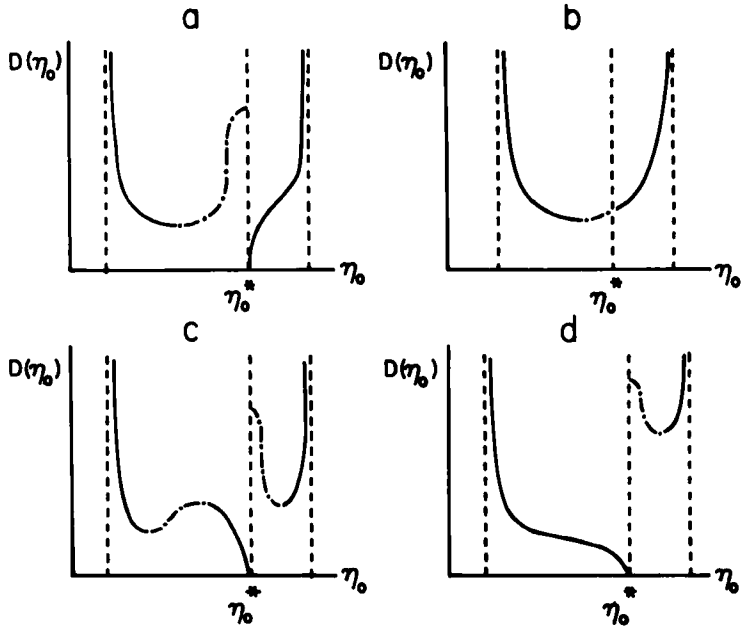

Figure 10. Graphs of $D(\eta_0)$, $g \neq 0$, case (ii(*b*)) in the text. (*a*) $t = t_{NI}$; (*b*) $t = t^* > t_{NI}$; (*c*) $t = t_1 > t^*$; (*d*) $t = t_{cr} > t_1$.

close to but slightly above the maximum of $F(\eta_0)$, and from equation (31) which gives D in terms of an integral between η_m and η_0. Thus we expect a qualitative change when η_{max}, which is an increasing function of t, reaches η_0^*, at a temperature t^* (cf. figure 10(*b*)). At η_0^* the governing equations are satisfied for arbitrary D, and

$$\lim_{\eta_0 \to \eta_0^{*-}} D(\eta_0) = \lim_{\eta_0 \to \eta_0^{*+}} D(\eta_0).$$

As t is increased further, η_0^* is now less than η_{max}, and so there is a region of instability on the right-hand branch of $D(\eta_0)$ (cf. figure 10(*c*)), and a region of what might still be called nematic stability (for small D) on the left-hand branch of $D(\eta_0)$. Finally (cf. figure 10(*d*)) the kink in the branch of $D(\eta_0)$ disappears at a critical point.

The profiles $\eta(z)$ corresponding to figure 10 are the same as those in figure 8 corresponding to case (ii(*a*)). Thus the profiles corresponding to figure 10(*a*) are shown in figure 9(*a*); the exceptional case corresponding to figure 10(*b*) is shown in figure 9(*b*), and figure 9(*c*) represents the profiles of figure 10(*c*).

We now consider case (iii) for which $\cos\theta < 0$, and $0 < \eta_0^* < \eta_c$. The surface disorder has now increased sufficiently to depress the ordering transition in a finite

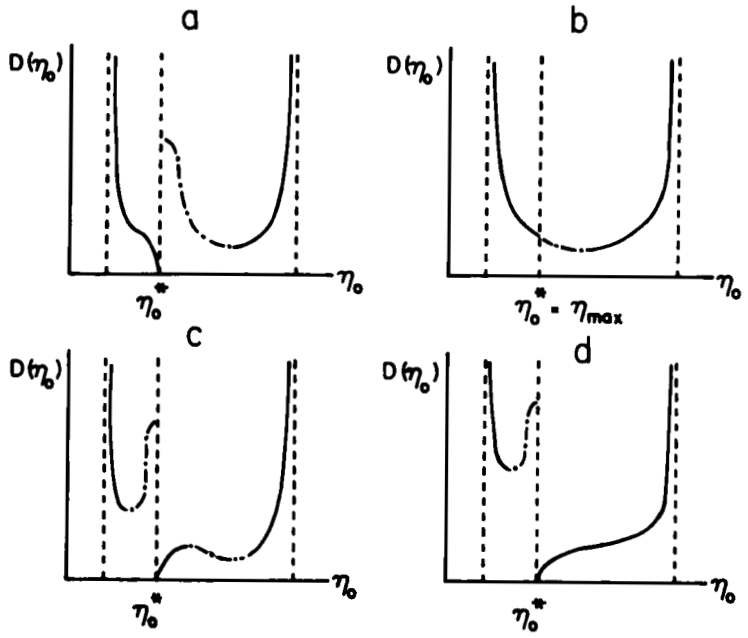

Figure 11. Graphs of $D(\eta_0)$, $\cos\theta < 0$. (*a*) $t = t_{NI}$; (*b*) $t = t^* < t_{NI}$; (*c*) $t = t_1 < t^*$; (*d*) $t = t_{cr} < t_1$.

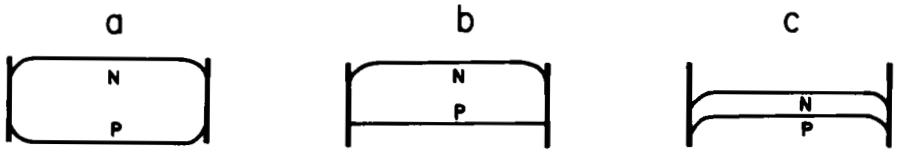

Figure 12. Coexisting profiles for case described in figure 11. (*a*) $t_{NI} > t > t^*$; (*b*) $t = t^*$; (*c*) $t^* > t > t_{cr}$.

system. The relevant region to examine is now $t < t_{NI}$. Graphs of $D(\eta_0)$ are shown, now in order of decreasing temperature, in figure 11. The features of this set of graphs are analogous to those of figure 10. Close to t_{NI} (cf. figure 11 (*a*)) $\eta_0^* < \eta_{max}$; there is a left-hand paranematic branch of $D(\eta_0)$ extending to $D = 0$ at η_0^*, and a right-hand nematic branch of $D(\eta_0)$ which becomes unstable close to η_0^* and terminates at a finite value of D at η_0^*. As t is decreased η_{max} decreases and reaches η_0^* (cf. figure 11 (*b*)), there is then an exchange of stability between the two branches and part of the paranematic branch lies to the right of η_0^* (cf. figure 11 (*c*)). Finally the kink in $D(\eta_0)$ disappears at a critical point (cf. figure 11 (*d*)).

The coexisting profiles corresponding to these graphs are shown in figure 12. In figure 12 (*a*), near t_{NI}, as in the previous cases there is a nematic phase slightly disordered near the wall and a paranematic phase ordered close to the wall, corresponding to figure 11 (*a*). Figure 12 (*b*) corresponds to the situation in figure 11 (*b*); for sufficiently small D the paranematic profiles have $\eta(z) = \eta_0^*$. Then the coexisting profiles in figure 12 (*c*) are both less ordered near the wall; this is consistent with both profiles corresponding to η_0 on the right hand branch of $D(\eta_0)$.

Finally we come to the case $h_1 = 0$, when the surface is purely disordering. Depending on the value of g the isotropic phase wets one wall partially

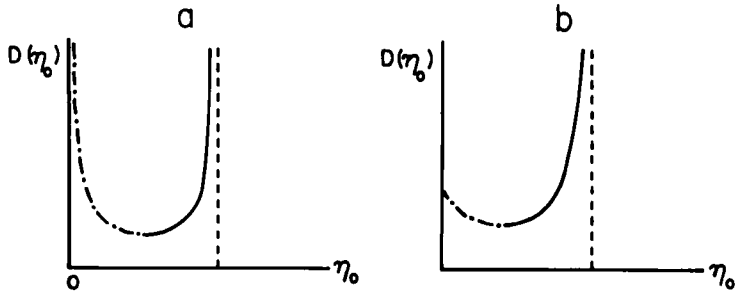

Figure 13. Graphs of $D(\eta_0)$ for a disordering surface $h_1 = 0$. (*a*) $0 < t < t_{NI}$; (*b*) $t < 0$.

$(-1 < \cos\theta < 0)$ or completely $(\cos\theta = -1)$. Complete wetting occurs if $g > \frac{1}{3}$. Plots of $D(\eta_0)$ for $0 < t < t_{NI}$ and $t < 0$ are shown in figure 13 (*a*) and (*b*), respectively. For $0 < t < t_{NI}$ there are two solutions: $\eta_0 = \eta_m = 0$ and a second solution which is the stable branch of $D(\eta_0)$. For complete wetting the right-hand asymptote approaches $\eta_0 = 0$ as $t \to t_{NI}^-$. From figure 13 (*a*) it is clear that there is no critical point for $t > 0$. For $t < 0$, $D(\eta_0)$ is finite and $D'(\eta_0)$ is negative. There is thus no critical point here either, except in the purely formal limit of $t_{cr} = -\infty$, at which $D(\eta_0 = 0) = 0'(\eta_0 = 0) = 0$. We remark that below $t = 0$ the bulk isotropic phase is unstable. However for a finite system with low enough D, the $\eta(z) = 0$ phase can be stabilized, even though it corresponds to a local maximum of $F(\eta)$, because then $\sigma = 0$.

References

[1] Poniewierski, A., and Sluckin, T. J., 1984, *Molec. Crystals liq. Crystals*, **111**, 143; 1985, *Molec. Crystals liq. Crystals*, **126**, 373.
[2] Sluckin, T. J., and Poniewierski, A., 1986, *Fluid Interfacial Phenomena*, edited by C. A. Croxton (John Wiley), p. 215.
[3] Sheng, P., 1976, *Phys. Rev. Lett.*, **37**, 1059; 1982, *Phys. Rev.* A, **26** 1610.
[4] Telo da Gama, M. M., 1984, *Molec. Phys.*, **52**, 585; 1984, *Molec. Phys.*, **52**, 611.
[5] See, for example, Sullivan, D. E., and Telo da Gama, M. M., 1986, *Fluid Interfacial Phenomena*, edited by C. A. Croxton (John Wiley), p. 45.
[6] Kuzma, M., and Labes, M. M., 1983, *Molec. Crystals liq. Crystals*, **100**, 103.
[7] Yokoyama, H., Kobayashi, S., and Kamei, H., 1985 (preprint).
[8] Thomson, W. T. (Lord Kelvin), 1871, *Phil. Mag.*, **42**, 448.
[9] Nakanishi, H., and Fisher, M. E., 1981, *J. chem. Phys.*, **75**, 5857.
[10] Lipowsky, R., and Gompper, G., 1984, *Phys. Rev.* B, **29**, 5213.
[11] Sornette, D., 1985, *Phys. Rev.* B, **31**, 4672.
[12] Evans, R., Marini Bettolo Marconi, U., and Tarazona, P., 1986, *J. chem. Phys.*, **84**, 2376.
[13] See, for example, Derjaguin, B. V., 1954, *Discuss. Faraday Soc.*, **18**, 26.
[14] Perez, E., Proust, J. E., and Ter-Minassian-Saraga, L., 1977, *Colloid polym. Sci.*, **255**, 1133; 1978, *Colloid polym. Sci.*, **256**, 784 (these articles are peculiar in that the first of these is No. 2 in the series, while the second is No. 1).
[15] Horn, R. G., Israelachvili, J. N., and Perez, E., 1981, *J. Phys., Paris*, **42**, 39.
[16] Kurik, M. V., 1977, *Fizika tverd. Tela*, **19**, 1849; 1977, *Soviet Phys. solid St.*, **19**, 1081; this equation was used to understand crystallization in a slab geometry.
[17] Fan, C. P., and Stephen, M. J., 1970, *Phys. Rev. Lett.*, **25**, 500.
[18] See also: Palffy-Muhoray, P., and Dunmur, D. A., 1983, *Molec. Crystals liq. Crystals*, **97**, 337. Wojtowicz, P. J., and Sheng, P., 1974, *Phys. Lett.* A, **48**, 235.
[19] The notation we adopt is consistent with that in the statistical mechanics literature; see, for example, Fisher, M. E., and Nakanishi, H., 1982, *Phys. Rev. Lett.*, **49**, 1565; the temperature variable is t and the surface fields are h_1 and g. For translation: Sheng's g [3] is essentially our h_1, Lipowsky and Gompper's [10] a_1 is our g, and Fan and Stephen's β [17] is our t.

[20] These results are in slight disagreement with those of Sheng [3]. For $g = 0$ we find t_{cr} weakly decreasing with h_1, although independent in the simple approximation. By contrast Sheng [3] finds t_{cr} increasing with h_1. The effects are, however, small.

[21] If we translate the notation of Sheng [3], we obtain for the parameters in equation (18): $A^1 = 8{\cdot}67 \times 10^4\,\mathrm{J\,m^{-3}\,K^{-1}}$, $B = 2{\cdot}12 \times 10^6\,\mathrm{J\,m^{-3}}$, $C = 1{\cdot}74 \times 10^6\,\mathrm{J\,m^{-3}}$, $T^* = 307{\cdot}14\,\mathrm{K}$, $L = 4{\cdot}5 \times 10^{-12}\,\mathrm{J\,m^{-1}}$, $\xi = 13{\cdot}2\,\text{Å}$.

[22] DE GENNES, P. G., 1981, *J. Phys Lett., Paris*, **42**, 377.

[23] MARČELJA, S., and RADIĆ, N., 1976, *Chem. Phys. Lett.*, **42**, 129.

[24] See, for example, GRIMSON, M. J., RICKAYZEN, G., and RICHMOND, P., 1980, *Molec. Phys.*, **39**, 61.

[25] GINZBURG, V. L., 1960, *Soviet Phys. solid St.*, **2**, 1824.